Time-Resolved Light Scattering Studies on Kinetics of Phase Separation and Phase Dissolution of Polymer Blends. 4. Kinetics of Phase Dissolution of a Binary Mixture of Polystyrene and Poly(vinyl methyl ether)†

Jiro Kumaki‡ and Takeji Hashimoto*

Department of Polymer Chemistry, Faculty of Engineering, Kyoto University, Kyoto 606, Japan. *Received May 31, 1985*

ABSTRACT: The kinetics of phase separation and phase dissolution for a polymer mixture (polystyrene and poly(vinyl methyl ether)) in the liquid state was studied by a time-resolved light scattering technique. The mixture, which has a LCST, was first demixed in thermodynamically metastable or unstable states for short periods of time to generate concentration fluctuations relevant to the early stage of phase separation. The mixture was then rapidly transferred to a thermodynamically stable state by the temperature-drop technique, and the decay rate $R(q)$ of the concentration fluctuations was investigated as a function of q, the wavenumber of the fluctuations. In early stages of dissolution in the small-q region, the concentration fluctuations decay approximately exponentially at a rate $R(q)$ proportional to q^2.

I. Introduction

Studies on phase-separation kinetics of polymer mixtures are of current interest.[1-17] Practically, such studies are important to design processability, morphology, and properties of polymer blends. From an academic viewpoint it is important to understand the effect of the connectivity of monomeric units, corresponding to atoms or molecules in metallic alloys, inorganic glasses, and organic liquids, on the time evolution of demixed structures. This problem is fundamental in nonequilibrium statistical physics.

Phase-dissolution kinetics of mixtures is also a subject of practical and academic interest. Here mixtures are first subjected to phase separation to some intermediate stage in either a thermodynamically unstable or a metastable state. The mixtures are then brought into a thermodynamically stable state and the kinetics of the thermally induced dissolution of the demixed structures is observed as a function of $\Delta T = T_s - T_x$, where T_s and T_x are the spinodal temperature for the mixture and the phase-dissolution temperatures of the mixture, respectively.

In this paper we employed a mixture of polystyrene (PS) and poly(vinyl methyl ether) (PVME) at an off-critical composition as a model system. Early stages of demixed structures were first developed by isothermal phase separation in the metastable or unstable state. The demixed structures were then isothermally dissolved by bringing the systems into the stable state. The dissolution kinetics was followed in real time by a time-resolved light scattering technique. In this paper we present preliminary results on the phase-dissolution kinetics and indicate some problems to be solved in the future.

II. Experimental Technique

1. Specimens. The PVME used in this study had a number-average molecular weight $M_n = 4.6 \times 10^4$ measured by membrane osmometry, and a heterogeneity index $M_w/M_n = 2.7$ measured by GPC. The PS had $M_n = 1.51 \times 10^5$ and $M_w/M_n = 1.4$. The polymer films, about 150 μm thick, were prepared by casting from 10 wt % toluene solutions of the mixture containing 30 vol % PVME and 70 vol % PS (designated as SE-30). The solvent-cast films, which were observed to be homogeneous,[18,19] were further heat-treated in a vacuum oven at 65 °C (well below the cloud point $T_{cl} = 106.5$ °C but well above the glass transition temperature $T_g = 23$ °C) for at least 24 h.

2. Methods. Figure 1 shows (a) definitions of various temperatures and (b) the thermal program employed in these studies. The films annealed in the vacuum oven were further annealed at the phase dissolution temperature T_x ($T_g < T_x < T_{cl}$). The scattered intensity profile $I_H(q)$ from the homogeneous mixture at $T = T_x$ was first measured with an automated light scattering photometer described previously.[8,20] Here q is the scattering vector magnitude defined by

$$q = (4\pi/\lambda) \sin (\theta/2) \tag{II-1}$$

where λ is the wavelength of incident light in the medium and θ is the scattering angle in the medium.

The film specimens were then subjected to a temperature jump to T_p, above the cloud point, where the mixtures underwent isothermal phase separation for a certain period of time t_p. The temperature T_p was set at either T_{p1} or T_{p2}, below and above T_s, respectively. During the time t_p, the kinetics of the isothermal phase separation were followed by the time-resolved scattering technique described earlier.[8,14] The film specimens, which were subjected to different extents of demixing at relatively early stages in the phase separation process by adjusting the time interval t_p, were then rapidly quenched to slightly below T_g for a short period of time t_i (a few minutes), long enough to prepare for the investigation of phase-dissolution kinetics at T_x. After the temperature of the sample was increased to T_x, the change of the scattering profile with time $I(q,t)$ was then measured with an automated light scattering photometer.[8,20]

III. Theoretical Background

In this section we consider *semiquantitatively* the theoretical aspects of the decay of the concentration fluctuations and the elastic scattering profiles involved in the phase-dissolution process.

Let us define the volume fractions of A and B segments to be ϕ and $(1 - \phi)$, respectively, at a given time and spatial position $\mathbf{r}$. The variation of the concentration fluctuations $\phi(\mathbf{r},t)$ with time during the initial dissolution process is given by a continuity equation

$$-\partial\phi/\partial t = \text{div } \mathbf{J}_A \tag{III-1}$$

where $\mathbf{J}_A$ is the diffusional flux of segment A. The diffusional flux is generated by thermodynamic driving forces $\nabla\mu_k$ (k = A, B)

$$\mathbf{J}_A = -(\Lambda_{AA}/k_BT)\nabla\mu_A - (\Lambda_{AB}/k_BT)\nabla\mu_B \tag{III-2a}$$

$$\mathbf{J}_B = -(\Lambda_{BA}/k_BT)\nabla\mu_A - (\Lambda_{BB}/k_BT)\nabla\mu_B \tag{III-2b}$$

† Presented in part before the 30th Annual Symposium of Polymer Science, Society of Polymer Science, Japan, Oct 1981. Kumaki, J.; Hashimoto, T.; Kawai, H. *Polym. Prepr. Jpn.* **1981**, *30*, 2102–2105.

‡ Present address: Research and Development Corp. of Japan, Sophia University, 7-1 Kioi-cho, Chiyoda-ku, Tokyo 102, Japan.

0024-9297/86/2219-0763$01.50/0

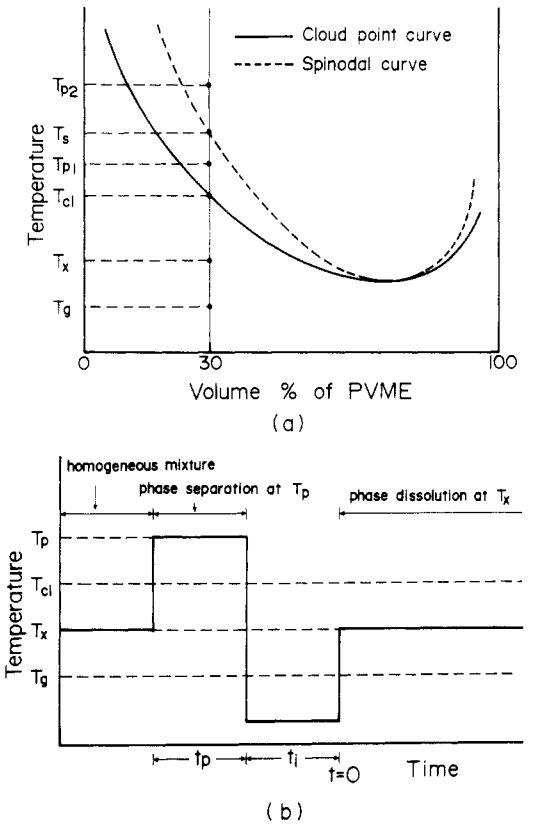

Figure 1. (a) Definitions of various temperatures used in this work and (b) temperature program for the studies on phase-dissolution kinetics.

where the Λ's are the Onsager coefficients. Incompressibility of the mixture invokes the requirement

$$\mathbf{J}_A + \mathbf{J}_B = 0 \tag{III-3}$$

which leads to

$$\Lambda_{AA} + \Lambda_{BA} = 0 \tag{III-4a}$$

$$\Lambda_{AB} + \Lambda_{BB} = 0 \tag{III-4b}$$

Onsager's reciprocal relation gives

$$\Lambda_{BA} = \Lambda_{AB} \tag{III-5}$$

and if

$$\Lambda \equiv \Lambda_{AA} \tag{III-6}$$

then

$$\Lambda_{BA} = \Lambda_{AB} = -\Lambda; \qquad \Lambda_{BB} = \Lambda \tag{III-7}$$

One thus obtains

$$\mathbf{J}_A = -(\Lambda/k_BT)\nabla(\mu_A - \mu_B) \tag{III-8}$$

From eq III-1 and 8, one then has

$$\partial\phi/\partial t = (\Lambda/k_BT)\nabla^2(\mu_A - \mu_B) \tag{III-9}$$

The Onsager coefficient generally depends on q in Fourier space,[4,5] where q is the wavenumber of the concentration fluctuations. However, we consider here only the limit of $q = 0$, for reasons to be discussed later. The thermodynamic potential $(\mu_A - \mu_B)$ may be calculated from the free energy functional $F(\{\phi\})$

$$\delta F = (\partial F/\partial\phi_A)\delta\phi_A + (\partial F/\partial\phi_B)\delta\phi_B = (\mu_A - \mu_B)\delta\phi \tag{III-10}$$

If F is given by adding the excess free energy due to fluctuations to the free energy of the uniform mixture described by the Flory–Huggins lattice model[21] in the form given by de Gennes,[4,30] then

$$F/k_BT = [\phi \ln \phi + (1 - \phi) \ln (1 - \phi)]/N + \chi\phi(1 - \phi) + \frac{a^2}{36\phi(1 - \phi)}(\nabla\phi)^2 \tag{III-11}$$

where F is the free energy per lattice site and a is Kuhn's statistical segment length, which is assumed for simplicity to be identical for polymers A and B. Then $(\mu_A - \mu_B)$ is given by

$$(\mu_A - \mu_B)/k_BT = \delta(F/k_BT)/\delta\phi = \frac{1}{N}\ln\frac{\phi}{1 - \phi} + \chi(1 - 2\phi) - \frac{a^2}{18\phi(1 - \phi)}\nabla^2\phi_A \tag{III-12}$$

For purposes of our preliminary studies, the terms related to gradient free energies $(\nabla\phi)^2$ and $\nabla^2\phi$ in eq III-11 and III-12, respectively, will be neglected in the following discussion. Some qualitative justification of this step is given in the next section. It is also assumed in eq III-11 that A and B polymers have the same degree of polymerization $N_A = N_B = N$ and χ is independent of ϕ.[27] Taking the gradient on both sides of eq III-12 and neglecting the term associated with the gradient free energy term $\nabla^2\phi$ in eq III-12, one obtains

$$\frac{\nabla^2(\mu_A - \mu_B)}{k_BT} = \left[\frac{1}{N\phi(1 - \phi)} - 2\chi\right]\nabla^2\phi + (\text{nonlinear terms}) \tag{III-13}$$

and from eq III-9 and 13, then

$$\frac{\partial\phi}{\partial t} = \Lambda\left[\frac{1}{N\phi(1 - \phi)} - 2\chi\right]\nabla^2\phi \tag{III-14}$$

Considering the q-Fourier component of fluctuations in eq III-14

$$\phi_q(\mathbf{r},t) = \phi_q(t)\exp(i\mathbf{q}\cdot\mathbf{r}) \tag{III-15}$$

and noting that

$$\nabla^2\phi_q(\mathbf{r},t) = -q^2\phi_q(\mathbf{r},t) \tag{III-16}$$

we have

$$\frac{1}{\phi_q}\frac{d\phi_q}{dt} = -q^2\Lambda\left[\frac{1}{N\phi(1 - \phi)} - 2\chi\right] \tag{III-17}$$

We restrict our arguments to the small-q regime,[24] satisfying $qR_0 \ll 1$, where R_0 is the individual polymer coil size. A de Gennes scaling argument[4] gives

$$\Lambda = N\phi(1 - \phi)D_c \tag{III-18}$$

under this criterion, where D_c is the diffusivities of polymer A and B and ϕ here refers to the *average* concentration of one component in the mixture, independent of the spatial coordinate. From eq III-17 and III-18 it follows that

$$\phi_q(t) = \phi_q(t=0)\exp[-R(q)t] \tag{III-19}$$

where

$$R(q) = q^2D_{app} \tag{III-20}$$

D_{app} is the apparent diffusivity as defined by

$$D_{app} \equiv D_c(\chi_s - \chi)/\chi_s \tag{III-21}$$

and χ_s is the χ-parameter at the spinodal point

$$\chi_s^{-1} = 2N\phi(1 - \phi) \tag{III-22}$$

which is given from the criterion that

$$\partial^2F/\partial\phi^2 = 0 \tag{III-23}$$

at the spinodal point. Thus the apparent diffusivity is D_c

Table I
Estimated Apparent Diffusivity D_{app} for the Phase-Dissolution Process

conditions for phase separation	phase dissolution temp, °C	$D_{app} \times 10^{13}$, cm^2/s	remarks
109 °C, 20 min	95.5	3 ± 1	demixing by
	85.5	1.2 ± 0.5	spinodal
	76	0.8 ± 0.1	decomposition
	66.3	0.5 ± 0.2	
106.5 °C, 113 min	85.5	1.7	demixing by
106.5 °C, 50 min	65	0.2	nucleation
106.5 °C, 40 min	60	0.07	and growth

times $(\chi_s - \chi)/\chi_s$, the thermodynamic driving force for the phase dissolution. The quantity $\phi_q(t=0)$ is the concentration fluctuation at time $t = 0$.

The exponential decay of the concentration fluctuations as given by eq III-15 predicts also the exponential decay of the scattered intensity

$$I_{theor}(q,t) = I_{theor}(q,t=0) \exp[-2R(q)t] \quad \text{(III-24)}$$

Thus, the linearization approximation in eq III-14 leads to exponential decay of the concentration fluctuations and the elastic scattered intensity at rates $R(q)$ and $2R(q)$, respectively. The neglect of the nonlocality of the interactions and of nonlinear terms and limitation of the observations to the small-q regime ($qR_0 \ll 1$) lead to the q dependence of $R(q)$ as given by eq III-20. In this context $R(q)$ should be proportional to q^2 and should depend on diffusivity D_c and thermodynamic driving force for the phase dissolution, $(\chi_s - \chi)/\chi_s$.

IV. Critique on the Assumptions

Among the various assumptions introduced to obtain eq III-19, III-20, and III-24, the following may be the most important: (i) neglect of the nonlocal interaction in the free energy of the fluctuating system (the term related to $(\nabla\phi)^2$ in eq III-11), (ii) the assumption of small q, giving rise to eq III-18, and (iii) the neglect of the nonlinear terms in eq III-13.

Assumptions i and ii are interrelated. The inclusion of the nonlocal entropic interactions (the term proportional to $\nabla^2\phi_A$ in eq III-12) results in the decay rate $R(q)$

$$R(q) = D_c q^2[(\chi - \chi_s)/\chi_s + (R_0^2/36)q^2] \quad \text{(IV-1)}$$

Since R_0 is the order of 100 Å and in this work $q < 10^5$ cm^{-1} (see data in section V), then $R_0^2 q^2 < \mathcal{O}(10^{-2})$. Thus the criterion of the small-q regime (ii) is satisfied. Moreover, $(\chi_s - \chi)/\chi_s \simeq (T_s - T_x)/T_x > 0.03$ since $T_s = 380$ K (see section V) and $T_x \lesssim 368.5$ K (see Table I and Figure 8). Consequently under the small-q regime covered in this work

$$(R_0^2/36)q^2 \ll (\chi - \chi_s)/\chi_s \quad \text{(IV-2)}$$

Consequently the gradient free-energy term may be neglected in this work. Neglect of this term should at least suffice for qualitative analysis of our preliminary data.

In the case of phase-separation kinetics, the nonlinear terms become increasingly important with time, because the order parameter $\Delta\phi(\mathbf{r},t) = \phi(\mathbf{r},t) - \phi_0$ increases with time (ϕ_0 being the average composition of one component). On the contrary, in the case of phase-dissolution kinetics, the nonlinear terms should be most important in the beginning and become less important with time. In this work, the initial concentration fluctuations were controlled to be very small by quenching the demixing at T_p in the very early stage of the phase separation (see Figure 1). Hence the nonlinear terms may not be significant from the beginning of the phase dissolution, and our initial analyses are based upon this assumption. It is our primary objective in this paper to check qualitative predictions based upon the simplified model.

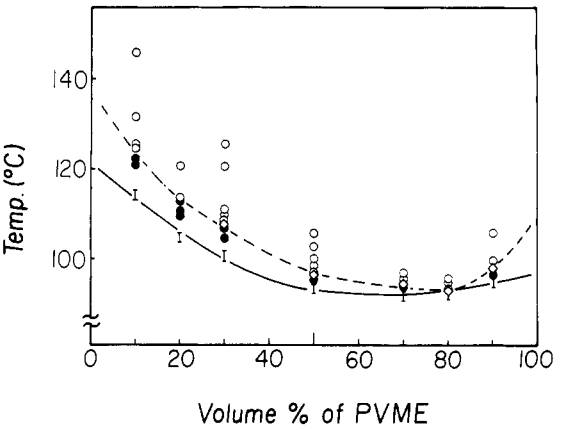

Figure 2. Phase diagram of PS/PVME mixture used in this study. The solid line corresponds to the cloud-point curve and the broken line corresponds to the spinodal curve determined by the dynamic method. The open and filled circles are the points where the phase separation occurs according to spinodal decomposition and nucleation–growth, respectively, as determined by time-resolved light scattering.

V. Results and Discussion

In this section we present some preliminary results on the phase-dissolution kinetics of the mixtures subjected to demixing in the early stage, and the results are analyzed on the basis of the semiquantitative theory presented in eq III-20 to III-24.

1. Phase Diagram. Figure 2 shows the phase diagram of PVME/PS binary mixtures. The solid line is the cloud-point curve, measured by change of scattered intensity at $\theta = 30°$ upon elevating temperature at a rate of 4 °C/h. The broken curve is the spinodal curve, measured by the dynamic method[8,14] with the time-resolved light scattering technique. The method involves determination of the apparent diffusivity D_{app} for phase separation as a function of quench depth

$$D_{app} \equiv -M(\partial^2 F/\partial\phi^2) \quad \text{(V-1a)}$$

$$= D_c(\chi - \chi_s)/\chi_s \quad \text{(V-1b)}$$

where M is a mobility constant, $M = \Lambda/k_B T$. Th spinodal point is determined as the point where D_{app} approaches zero as shown in the small insert in Figure 3.

The open circles in Figure 2 are the points at which the demixing produced by the temperature jump shows definitely exponential increase of the scattered intensity with time *in the initial stage of the phase separation*, as shown in Figure 3 for the demixing at temperatures higher than 107 °C. This observation confirms demixing by spinodal decomposition.[8,25] On the other hand, the filled circles are the points at which demixing produced by the temperature jump definitely shows nonexponential increase of the scattered intensity with time *from the very beginning of the phase separation*, as shown in Figure 3 for demixing at temperatures 106 and 104 °C. This observation confirms demixing according to nucleation and growth.[26] The cloud point thus estimated was 101.5 ± 0.5 °C and the spinodal point was 107.2 °C for 70/30 (v/v) PS/PVME.

2. Phase-Dissolution Kinetics. Phase-dissolution kinetics were studied for the specimens demixed at $T_{p2} = 108.5$ °C for 20 min according to spinodal decomposition and for those demixed at $T_{p1} = 106$ °C for 40–113 min according to nucleation and growth. The former demixing

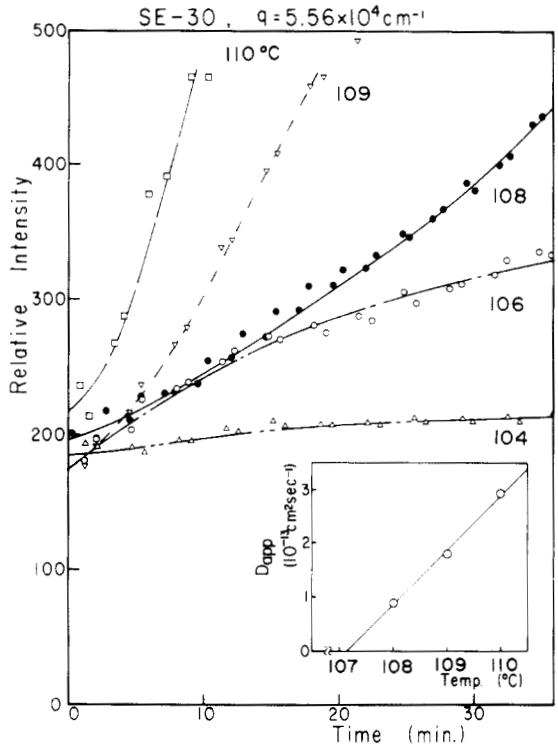

Figure 3. Change of the scattered intensity at $q = 5.56 \times 10^4$ cm^{-1} with time during the early stages of the isothermal phase separation for PS/PVME. Note that the spinodal temperature was estimated to be $T_s = 107.2$ °C from plots of apparent diffusivity for the phase separation as a function of temperature as shown in the small diagram inserted in this figure. At $T > T_s$, the scattered intensity exponentially increases with time, but at $T < T_s$ the intensity increase is nonexponential.

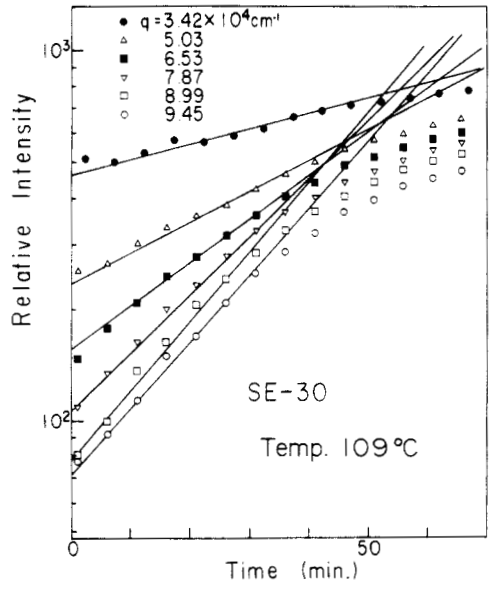

Figure 4. Change of scattered intensities at various q's with time during the isothermal phase separation at 109 °C. Note that the intensities increase exponentially with time up to about 30 min after the onset of the phase separation.

at T_{p2} for 20 min corresponds to an early stage of the spinodal decomposition, as clearly shown in Figure 4; the scattered intensities at various q's increase exponentially with time up to about 30 min.

Figures 5 and 6 show typical decays of the scattered intensities at various q's for phase dissolutions at 65 and 85.5 °C, respectively, for the demixed mixtures at T_{p1}. Here the measured scattered intensity $I(q,t)$ at T_x was corrected for the scattered intensity in the stable state

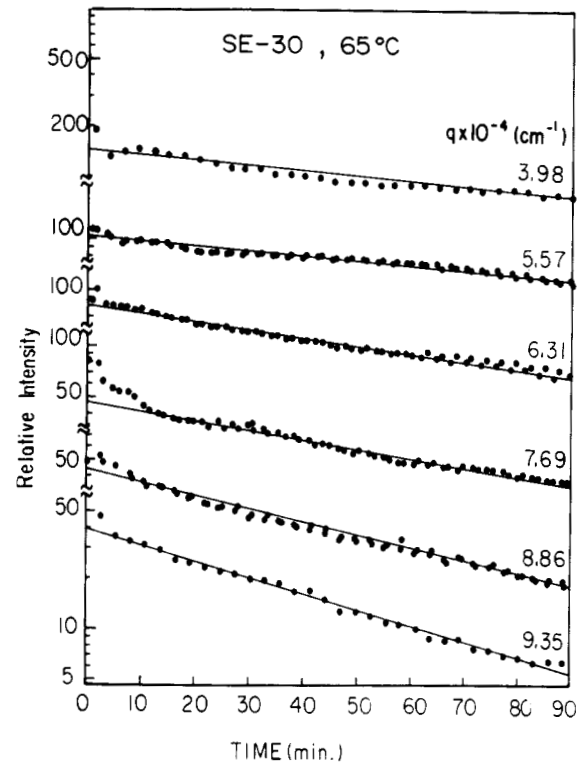

Figure 5. Decay of the corrected scattered intensities I_{corr} at various q's during the isothermal phase-dissolution process at 65 °C for the mixtured demixed at 106.5 °C for 50 min.

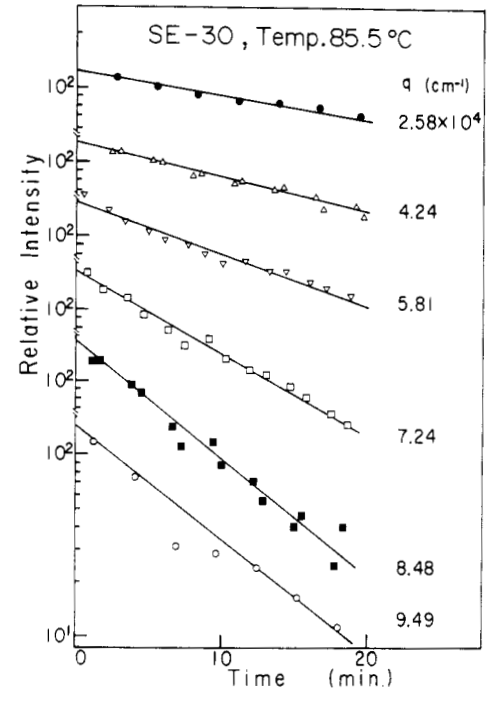

Figure 6. Decay of the corrected scattered intensities I_{corr} at various q's during the isothermal phase-dissolution process at 85.5 °C for the mixture demixed at 106.5 °C for 113 min.

$I_H(q)$ at T_x in order to facilitate the analysis based on eq III-24.

$$I_{corr}(q,t;T_x) = I(q,t;T_x) - I_H(q;T_x) \quad \text{(V-2)}$$

The correction leads to

$$\lim_{t\to\infty} I_{corr}(q,t;T_x) = 0 \quad \text{(V-3a)}$$

$$\lim_{t\to 0} I_{corr}(q,t;T_x) = I_{corr}(q,t=0;T_x) = I(q,t=0;T_x) - I_H(q;T_x) \quad \text{(V-3b)}$$

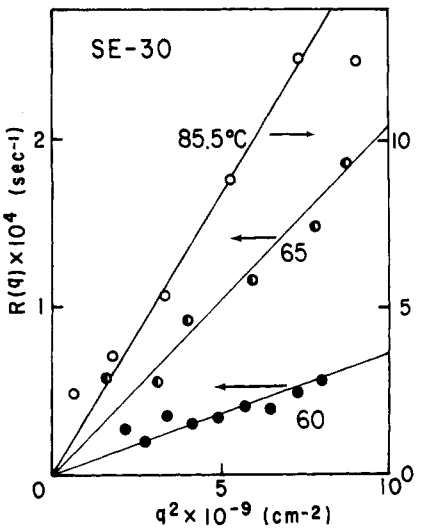

Figure 7. Decay rate $R(q)$ of the concentration fluctuations as a function of q^2 for the dissolutions at 60, 65, and at 85.5 °C for the mixtures demixed by nucleation and growth.

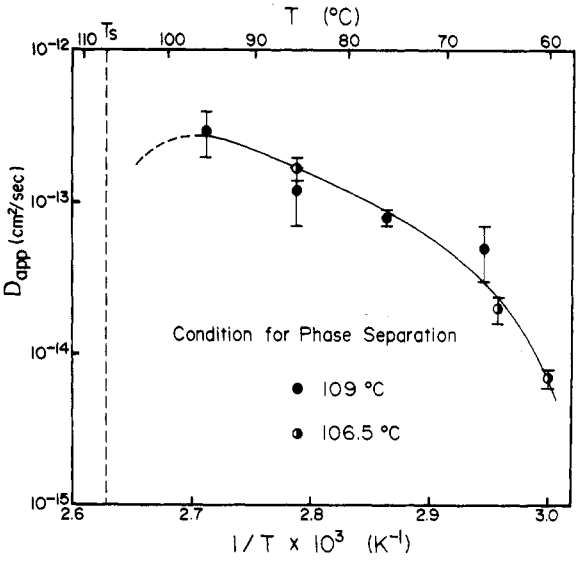

Figure 8. Estimated apparent diffusivity D_{app} for the dissolution process as a function of T (°C) or $1/T$ (K^{-1}).

and hence enables one to compare $I_{corr}(q,t)$ with $I_{theor}(q,t)$ in eq III-24. The ordinates in Figures 5, 6, and 9 correspond to $I_{corr}(q,t)$ in relative intensity scale.

The results presented in Figures 5 and 6 and also those at other temperatures show *approximately* an exponential decay of scattered intensity with time during phase dissolution, with a decay rate which depends on q. Similar trends were also observed for the phase dissolution from the samples demixed at T_{p2} for 20 min, except that fits with exponential decay curves for these samples were less satisfactory.

3. Theoretical Analysis. The decay rate of the scattered intensity $2R(q)$ and that of the concentration fluctuations $R(q)$ were determined from the slopes in the plots of Figures 5 and 6. The dependence of $R(q)$ on q is summarized in Figure 7 for dissolutions of samples demixed at T_{p1} (nucleation and growth). Although the data points are rather scattered, the data *qualitatively* indicate that $R(q)$ is proportional to q^2 in the small-q regime, as predicted from eq III-20.

By using eq III-20 one can estimate the apparent diffusivity D_{app} from the slopes of the plots, as shown in Figure 7. Estimated D_{app}'s are summarized in Table I and plotted in Figure 8 as a function of temperature. The apparent diffusivity decreases with decreasing temperature, and the two types of demixed samples exhibit almost identical trends. The decrease of D_{app} with decreasing T implies that the effect of decreasing D_c outweighs the effect of increasing thermodynamic driving force for the phase dissolution $(\chi_s - \chi)/\chi_s$ ("diffusion-controlled" regime). Although it is not supported by our experimental results so far, the broken curve is also included in the figure to indicate the possibility that there is a regime where D_{app} is controlled by the thermodynamic driving force $(\chi_s - \chi/\chi_s)$ for the phase dissolution.

VI. Concluding Remarks

We have described the dissolution kinetics for two kinds of mixtures, subjected to demixing according to spinodal decomposition and nucleation–growth in the early stage, and *in the small-q regime* (i.e., $QR_0 \ll 1$). The preliminary results indicate that the dissolution kinetics for the two kinds of mixtures are almost identical and independent of thermal history.

The isothermal dissolution process tends to produce approximately exponential decay of the scattered intensities and of the concentration fluctuations with time *in the small-q regime*, the decay rate of which is roughly proportional to q^2, as predicted in section III. However, more quantitative experimental results are definitely required to draw a final conclusion.

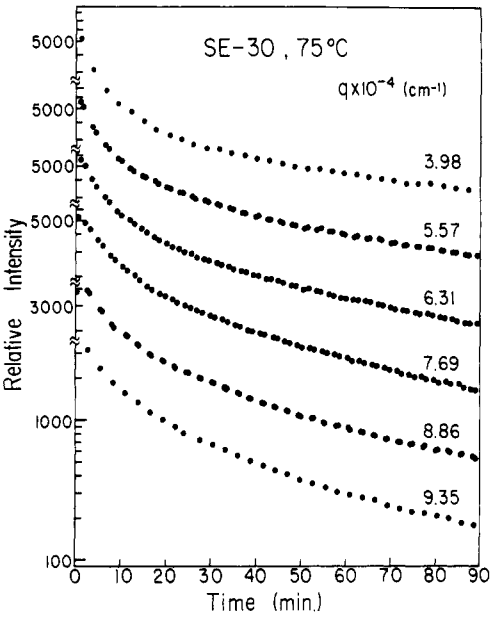

Figure 9. Decay of the corrected scattered intensities I_{corr} at various q's during the isothermal phase-dissolution at 75 °C for the mixture demixed at 121 °C for 20 min.

Further quantitative studies will be required for critical tests of the exponential decay and q^2 dependence of the decay rate, especially *in the high-q regime and for mixtures demixed to various stages*. For example, Figure 9 represents the decay of scattered intensities at various q's during the dissolution process at 75 °C for a mixture demixed at 121 °C for 20 min. The demixing process would here obviously generate structures relevant to a *late stage of spinodal decomposition*. Dissolution from such well-developed demised structure does not give exponential decay as in Figures 5 and 6 but rather shows nonexponential decay as indicated in the remarkable curvatures of ln I_{corr} vs. t. This point should receive further study. More theoretical work is also required to account rigorously for (i) the effect of free-energy gradient, which may become increasingly important with increasing q and (ii) the effect

of nonlinear terms which may become increasingly important in more advanced demixed states. Equations III-19 and III-24 indicate, respectively, that the concentration fluctuations completely disappear and that the scattered intensity goes to zero after a sufficient period of time. This is not correct, because there are thermal fluctuations even in homogeneous mixtures which causes elastic scattering equal to $I_H(q;T_x)$. A correction for this effect was made in eq V-2 and the corrected scattered intensity $I_{corr}(q,t)$ was compared with $I_{theor}(q,t)$ in eq III-24. A more rigorous theoretical treatment is obviously required, and the theory should allow $I_{theor}(q,t)$ to approch $I_H(q;T_x)$ at $t \rightarrow \infty$ by properly accounting for the thermal noise appropriate to the small-q regime.

Registry No. PS (homopolymer), 9003-53-6; PVME (homopolymer), 9003-09-2.

References and Notes

(1) van Aartsen, J. J. *Eur. Polym. J.* **1970**, *6*, 919.
(2) van Aartsen, J. J.; Smolders, C. A. *Eur. Polym. J.* **1970**, *6*, 1105.
(3) Nishi, T.; Wang, T. T.; Kwei, T. K. *Macromolecules* **1975**, *8*, 227.
(4) de Gennes, P.-G. *J. Chem. Phys.* **1980**, *72*, 4756.
(5) Pincus, P. J. *J. Chem. Phys.* **1981**, *75*, 1996.
(6) Nojima, S.; Tsutsumi, T.; Nose, T. *Polym. J.* **1982**, *14*, 225.
(7) Nojima, S.; Ohyama, Y.; Yamaguchi, M.; Nose, T. *Polym. J.* **1982**, *14*, 907.
(8) Hashimoto, T.; Kumaki, J.; Kawai, H. *Macromolecules* **1983**, *16*, 641.
(9) Snyder, H. L.; Meakin, P.; Reich, S. *Macromolecules* **1983**, *16*, 757.
(10) Gelles, R.; Frank, C. W. *Macromolecules* **1983**, *16*, 1448.
(11) Snyder, H. L.; Meakin, P. *J. Chem. Phys.* **1983**, *79*, 5588.
(12) Binder, K. *J. Chem. Phys.* **1983**, *79*, 6387.
(13) Hashimoto, T.; Sasaki, K.; Kawai, H. *Macromolecules* **1984**, *17*, 2812.
(14) Sasaki, K.; Hashimoto, T. *Macromolecules* **1984**, *17*, 2818.
(15) Inoue, T.; Ougizawa, T.; Yasuda, O.; Miyasaka, K. *Macromolecules* **1985**, *18*, 57.
(16) Russell, T. P.; Hadziioannou, G.; Warburton, W. K. *Macromolecules* **1985**, *18*, 78.
(17) Strobl, G. R. *Macromolecules* **1985**, *18*, 558.
(18) Bank, M.; Leffingwell, J.; Thies, C. *Macromolecules* **1971**, *4*, 43; *J. Polym. Sci., Polym. Phys. Ed.* **1972**, *10*, 1097.
(19) Nishi, T.; Kwei, T. K. *Polymer* **1975**, *16*, 285.
(20) Tanaka, K.; Saijo, K.; Suehiro, S.; Hashimoto, T.; Kawai, H. *Polym. Prepr. Jpn.* **1981**, *30*, 2094.
(21) Flory, P. "Principles of Polymer Chemistry", Cornell University Press: Ithaca, NY, 1971.
(22) Cahn, J. W.; Hilliard, J. E. *J. Chem. Phys.* **1958**, *29*, 258; **1959**, *31*, 688.
(23) Cahn, J. W. *J. Chem. Phys.* **1965**, *42*, 93.
(24) This restriction is reasonable since the q region covered by this light scattering method is $q < 10^5$ cm^{-1} and R_0 is the order of 10^{-6} cm and hence $qR_0 < 10^{-1}$.
(25) Izumitani, T.; Hashimoto, T. *J. Chem. Phys.* **1985**, *83*, 3694.
(26) The demixing in the unstable region for this particular mixture definitely involves the exponential growth of the scattered intensity with time over a sufficiently long time interval, and this time interval increases with decreasing quench depth. Hence the nonexponential growth observed at temperatures 106 and 104 °C, lower than T_s = 107 °C, i.e., at smaller quench depths, can be best interpreted as a manifestation of the nucleation and growth.
(27) Recent experiments of Shelten et al.[28] and Stein et al.[29] have shown that χ is a function of ϕ.
(28) Herkt-Maetzky, C.; Schelten, J. *Phys. Rev. Lett.* **1983**, *51*, 896.
(29) Yang, H.; Shibayama, M.; Stein, R. S.; Han, C. C. *Polym. Bull.* **1984**, *12*, 7. Shibayama, M.; Yang, H.; Stein, R. S.; Han, C. C. *Macromolecules* **1985**, *18*, 2179.
(30) The gradient free energy appearing on the right-hand side of eq III-11 originates from nonlocal entropic contributions to F rather than nonlocal energetic contributions. The nonlocal energetic contributions were neglected as they are small compared with the entropic contributions associated with connectivity of the segments. The nonlocal entropy contributions for polymer solutions were described by Vrij and van den Esker.[31]
(31) Vrij, A.; van den Esker, M. W. J. *J. Chem. Soc., Faraday Trans. 2* **1972**, *68*, 513.

Static Light Scattering Study of High Molecular Weight 18-Arm Star Block Copolymers

Anh B. Nguyen,[1a] Nikos Hadjichristidis,[1b] and Lewis J. Fetters*[1c]

Institute of Polymer Science, University of Akron, Akron, Ohio 44325.

Received August 23, 1985

ABSTRACT: Light scattering studies on very high molecular weight 18-arm star poly(styrene–isoprene) block copolymers have been done by using, in part, isorefractive solvents. The radius of gyration of the polystyrene outer blocks is expanded to approximately the same size as the whole macromolecule while that of the polyisoprene inner segment assumes the dimensions of a homopolyisoprene star of equivalent molecular weight and functionality. The shape of the polystyrene outer blocks resembles that predicted for a hollow star. The findings support the presence of a segregated vesicle-like conformation in dilute solution.

Introduction

The dilute solution conformational aspects of linear di- or triblock copolymers have been the subject of experimental[2-13] and theoretical[14-16] considerations. The architecture of copolymers containing homopolymer segments can influence their dilute solution conformation. An example of this behavior is seen in the model graft copolymer work of Rahlwes, Roovers, and Bywater[17] and Hadjichristidis and Roovers.[18] The latter authors, via the use of isorefractive solvents, reached the conclusion that intramolecular separation existed and that the conformation of the poly(isoprene-*g*-styrene) copolymer could be classified as a core-shell structure in dilute solution with the polyisoprene backbone preferentially occupying the core. In view of this latter result, it is apparent that the conformation of a star block copolymer could be studied in a similar fashion by measuring the apparent radii of gyration in isorefractive solvents. Furthermore, because of the anticipated "advantageous" geometry of star block copolymers, their conformation would be expected to be amenable to a shape analysis by an evaluation of the particle scattering factor. This dual approach applied to two high molecular weight 18-arm star block copolymers is the subject of this paper.

Experimental Section

Two high molecular weight star block copolymer materials were prepared in benzene. Dilute solutions, ≃2% (w/v), were adhered to in the polymerizations. The linking reaction, involving an

0024-9297/86/2219-0768$01.50/0